Genetic algorithm optimization of an opposition control strategy in a fully turbulent channel flow

GENETIC ALGORITHM OPTIMIZATION OF AN OPPOSITION CONTROL STRATEGY IN A FULLY TURBULENT CHANNEL FLOW

Enrico Saccaggi[1] & Gaetano Maria Di Cicca[1]

[1]Department of Mechanical and Aerospace Engineering, Politecnico di Torino, Corso Duca degli Abruzzi 24, Torino

Abstract

The proposed study investigates a real-time opposition control strategy to reduce the skin friction drag driven by a genetic algorithm optimization. The experiments are carried out in a fully turbulent channel flow having the friction Reynolds number $Re_\tau = 420$. Opposition control of sweep events is implemented using a wall-normal jet. Changes to the turbulence structure in the region closer to the wall are examined using hot-wire anemometry. By using a genetic algorithm, amplitude, frequency, and delay are optimized to minimize the sweep events intensity.

Keywords: aerodynamics, flow control, genetic algorithm, drag reduction, hot-wire anemometry

1. Introduction

The significance of drag reduction becomes essential to diminish both energy consumption and pollutant emissions in modern transportation systems. The transportation sector, accounting for the 25% of the energy budget, is responsible for more than the 10% of global greenhouse gasses as mentioned in Cheng et al. [3]. Skin friction stands out as a crucial contributor to drag, accounting for as much as 55% of the total drag for commercial aircraft.

Various techniques have been suggested in the past years to reduce the skin friction drag both experimentally and numerically (see e.g. [5], [10], and [14]). Most of the drag reduction strategies, focus on the coherent structures near the wall, such as quasi-streamwise vortices (QSVs) and velocity streaks, which are closely tied to skin-friction drag. Well-known events like ejections and sweeps are closely linked to QSVs [13]. Recent studies have demonstrated that near-wall turbulence events can be controlled using a relatively simple scheme, resulting in skin friction reductions.

Choi et al. [4] conducted direct numerical simulations of active control in turbulent channel flow. They found that applying blowing and suction to counteract the wall-normal velocities, skin friction reduction of up to 25% can be achieved. Additionally, they observed that drag is reduced when the detection plane is close to the wall ($y^+ \approx 10$), whereas drag significantly increases when the detection plane is farther from the wall.

Rebbeck and Choi [12] performed a wind tunnel experiment on real-time opposition control. They examined how the near-wall turbulence structure of the boundary layer changes when opposition control is applied to individual sweep events using a wall-normal jet. Their results indicated that the wall-ward movement of high-speed fluid during sweep events can be effectively blocked by a wall-normal jet produced by a loudspeaker actuator. This suggests that opposition control of wall turbulence can reduce the skin friction drag of the turbulent boundary layer.

More recently, Yu et al. [15] developed an artificial intelligence open-loop control system to manipulate a turbulent boundary layer over a flat plate, with the aim of reducing friction drag. The boundary layer is characterized by a Reynolds number based on a momentum thickness, Re_θ, equal to 1450. The system is constituted of synthetic jets, wall-wire sensors, and a genetic algorithm for the unsupervised learning of optimal control law. The velocity, frequency, and actuation phase of each synthetic jet (issuing from a rectangular streamwise slit) can be independently controlled. By using

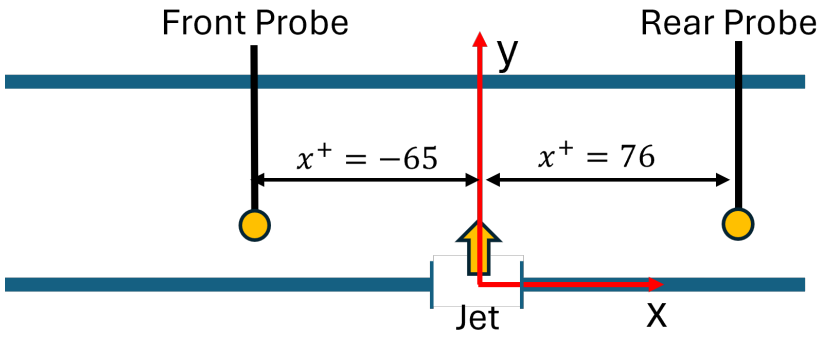

Figure 1 – Sketch of the experimental setup for the real-time opposition control. The air stream flows from left to right. The upstream probe is positioned at $x^+ = -65$, the rear probe is positioned at $x^+ = 76$. Both probes are placed at $y^+ = 15$.

artificial intelligence control to find optimized non-uniform forcing, a local drag reduction of up to 60% downstream of the synthetic jets has been observed, along with an extended effective drag reduction area compared to conventional open-loop control.
In the work of Castellanos et al. [2] a genetic algorithm control logic was applied to optimize the actuation parameters to maximize the convective heat transfer enhancement in a turbulent boundary layer. In that study a spanwise array of six slots jets were used as actuators. The study demonstrated the potential and applicability of machine learning control to explore the control space.
More examples and works of machine learning control logic applied in fluid dynamics can be found in the study of Noack [9].
In the present study, a real-time opposition control strategy with the aim of reducing skin friction drag is investigated. The experiments are conducted in a fully turbulent channel flow having the friction Reynolds number $Re_\tau = 420$. A genetic algorithm is used for the optimization of the jet actuation parameters (amplitude, frequency, and delay). Modifications of the near-wall turbulence structure in the boundary layer produced by this control strategy are examined.
Section 2 defines the experimental setup and the measurement techniques. Section 3 describes the genetic algorithm control setup and the expression for the cost function. The results are analysed in Section 4 and the conclusions in Section 5.

2. Experimental setup

The experiments were carried out in an 8-meter-long duct with a rectangular section 7 cm high and 30 cm wide. A velocity of $U_0 = 3.34\,\mathrm{m\,s^{-1}}$ in the center line was imposed. The friction velocity evaluated through the measured pressure gradient along the channel was $u_\tau = 0.185\,\mathrm{m\,s^{-1}}$ which leads to a friction Reynolds number $Re_\tau = 420$.
Two hot-wire probes are used in the present study, both of them connected to a Dantec 55M10 CTA Standard Bridge. The front probe (see Figure 1) is positioned upstream of the jet orifice at $x^+ = -65$ and at a wall-normal distance of $y^+ = 15$. The front probe is a Dantec 55P11 straight probe with a sensitive tungsten wire of $5\,\mu\mathrm{m}$ in diameter and $1.25\,\mathrm{mm}$ in length (equivalent to about 15 wall units).
In accordance with Rebbeck and Choi [11] detection of sweep events is obtained by applying the velocity gradient technique to the longitudinal component of the velocity u measured by the front probe. In a more precise way, the gradient is computed from the analog voltage output signal of the front probe by a differentiating device, and the sweep event is identified when the computed gradient exceeds a given threshold by a comparator device.
When the comparator device identifies a sweep event then a TTL signal is sent to the microcontroller, Arduino Uno Rev3 board. The purpose of the microcontroller is to delay the TTL signal to account for both the convection time between the front probe and the control point and the jet actuator system response time.
The TTL signal from the microcontroller triggers the signal generator (Agilent 33120A), to produce a sine wave with a given amplitude and frequency. The sine wave is sent to an amplifier (Kenwood

KAC-5205) that can drive the loudspeaker actuator and a jet, issuing from a $1\,\mathrm{mm}$ in diameter orifice, is produced.
In this work, amplitude, frequency, and delay were optimized through a genetic algorithm by maximizing sweep event velocity reduction over the whole episode. This quantity is obtained by measuring the velocity at a distance from the wall $y^+ = 15$ through the rear probe, positioned at $x^+ = 76$.
The downstream probe can be moved at different stream-wise distances from the orifice and was employed to observe modifications in the turbulence structure resulting from the opposition control in the region closer to the wall.
The rear probe used was a Dantec 55P15 boundary-layer probe, equipped with a sensitive tungsten wire measuring $5\,\mu\mathrm{m}$ in diameter and $1.25\,\mathrm{mm}$ in length. This probe is connected to a 2-axis movable stand to allow movement in the stream-wise direction x and the direction normal to the wall y. To allow the motion of this probe, the top plate of the channel has a slit which can be sealed during the measurements.
Both hot wire probes were calibrated in situ and the calibration curves were fitted with the King's law. Hot-wire signals were collected by a National Instruments PCI-MIO-16-XE-10 16-bit DAQ board at a sample rate of $10\,\mathrm{kHz}$. At the same rate, the TTL output signal from the microcontroller is also sampled.
The National Instrument acquisition board was placed inside the workstation, connected to the PCI bus. A microcontroller interfaces with the acquisition board via a USB-type serial port, while the function generator is linked to the workstation through an RS-232 serial port. For post-processing data and executing the genetic algorithm, a laptop is paired with the workstation via an Ethernet port, and they communicate using the TCP protocol. A server-based Python algorithm leveraging the Python's built-in socket library was loaded onto the workstation. A client-based script was written on the laptop instead.
Typically, the client (laptop) initiates a query to the server (workstation). This query could involve either a measurement or a policy change. After executing the command, the client requests feedback or a data buffer if a signal has been acquired. Finally, the laptop processes the raw signal.

3. Genetic algorithm-based control system

The control system depicted in Figure 2 comprises control hardware and control logic. The control hardware is responsible for detection and actuation, while the control logic, based on a genetic algorithm, iteratively adjusts the system's response.
A workstation primarily manages the control hardware, whereas the control logic is executed on a laptop. As illustrated in Figure 2, these devices are interconnected via a TCP connection.

3.1 Control Hardware

The control hardware is mainly composed of sensors (two hot-wire probes), an actuator (loudspeaker), a microcontroller, a differentiator, and a comparator which were partly described in Di Cicca [6]. This hardware can detect the sweep events and actuate the loudspeaker very quickly. As described in the previous paragraph, the detection of sweep events is obtained by applying the velocity gradient technique to the longitudinal component of the velocity u measured by the upstream hot-wire probe.
The microcontroller has been programmed with a circular buffer of a sufficiently large number of elements so that no events are missed. The connection through the serial interface allows the delay time to be changed once requested by the genetic algorithm.
In Figure 3, it can be observed how the signal was manipulated to detect the sweep events. The signal in blue represents the front probe velocity signal. The velocity gradient signal is evaluated in real-time (green-colored curve) and upon a comparison with a given threshold, events are identified (dashed red vertical line). To account for convection, the actuation is delayed at the points where the dashed orange vertical line is shown.

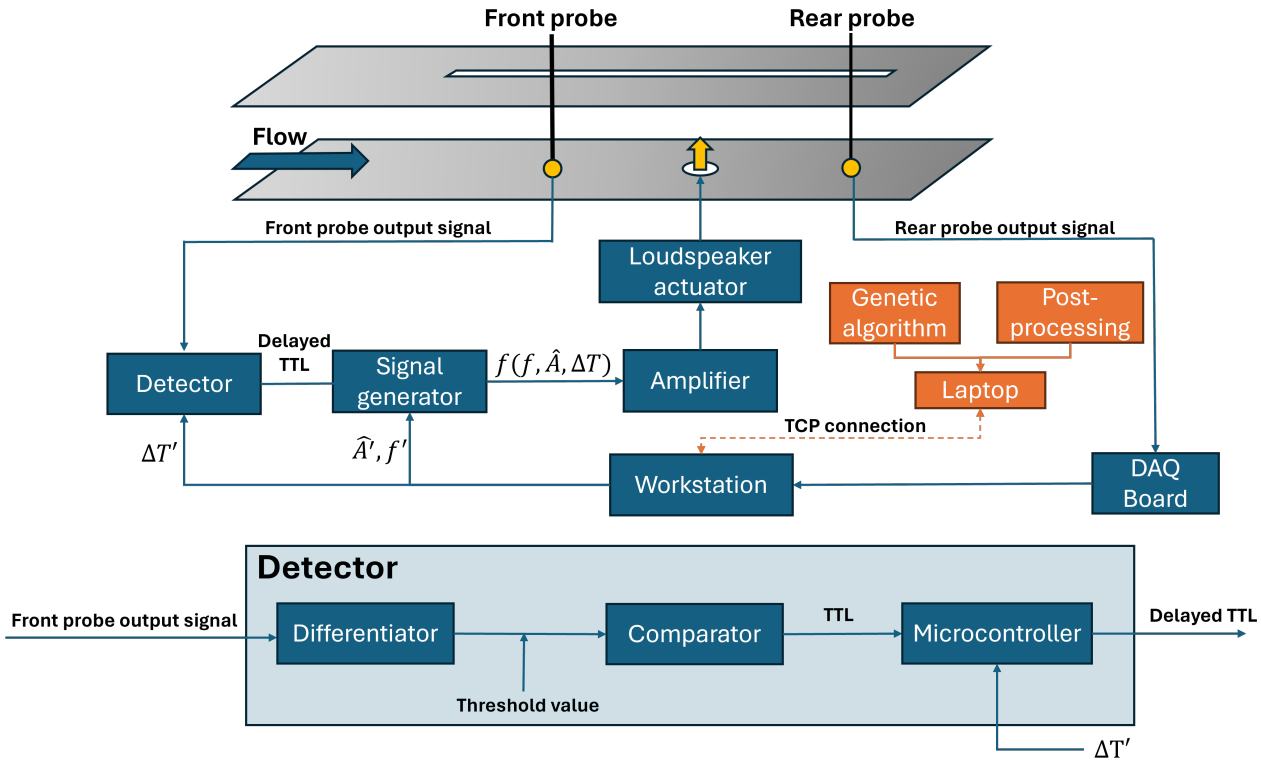

Figure 2 – Schematic of the control system. The signal from the upstream probe is used to trigger the actuation. The signal coming from the downstream probe is used to optimize the control strategy. $f, \hat{A}, \Delta T$ are respectively the frequency, the amplitude, and the delay time imposed on the actuator. The superscript $'$ indicates the updated value.

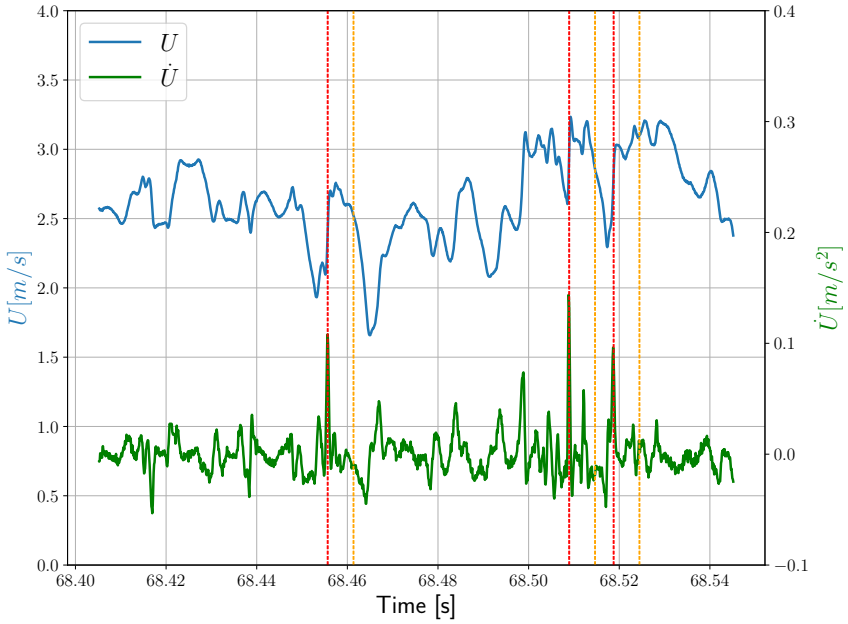

Figure 3 – Sweep events detection algorithm visualization. In blue is the longitudinal component of the front probe instantaneous velocity signal (U) and in green is its time derivative ($\dot{U}$). Red and orange vertical lines show the trigger instant and the delayed one respectively.

The comparator threshold level was adjusted to have a similar number of events both through the VITA (variable interval time averaging) technique (see Blackwelder and Kaplan [1]) and through the velocity gradient technique. The reference VITA technique parameters are a threshold value $k = 1.2$ and an averaging time $T^+ = 10$.
The output signal of the hot-wire probe placed downstream of the control point is instead used to evaluate the local mean velocity reduction averaged over the whole episode and to observe modifications in the turbulence structure resulting from the opposition control in the region closer to the wall.

3.2 Control parameters optimization using a Genetic Algorithm

A closed-loop control logic was implemented through a genetic algorithm. The goal of the control algorithm is to minimize the mean velocity in the averaged conditional event. To achieve this, the difference between the area subtended by the velocity curve in the controlled (A_c) and uncontrolled (A_nc) case was evaluated. The cost function $\mathcal{J}$ was computed with the following equation:

$$\mathcal{J}(\psi) = -\frac{A_\mathrm{nc} - A_\mathrm{c}(\psi)}{A_\mathrm{nc}}, \tag{1}$$

where the generic area in either controlled or uncontrolled cases is:

$$A = \int_{t_m}^{t_w} u^+ dt, \tag{2}$$

in which u^+ is the fluctuating component of the streamwise velocity in wall units, t_m is the time in correspondence of the first minimum peak, t_w is a time window that was selected to ensure the robustness of the cost function, ψ is a triplet consisting of voltage amplitude, frequency, and delay. In Figure 4, the conditional averaged sweep events are shown for the controlled and uncontrolled cases. The difference between the two areas (A_nc and A_c) and the box bounds (t_m and t_w) where the integral was computed can be observed.
The negative sign in Equation 1 was introduced since the difference between the uncontrolled and controlled area should be as large as possible but the cost function needs to be minimized.
An episode consists of a 120-second time interval in which amplitude, frequency, and delay are set constant. The episode length was calibrated to ensure a sufficient number of events for statistics (about 800). Finally, each generation is evaluated 2 more times to reduce uncertainty due to environmental and operational conditions at the facility.
The first generation ($n = 1$) of the genetic algorithm consists of $N_i = 6$ random ψ triplets (also called individuals). Once the interval boundaries have been defined, the population is initialized as follows: half with Gaussian distribution with mean and standard deviation defined by the boundaries of the interval and half uniformly distributed. For each individual "*i*", a 120-second episode is set three times, and the cost function $\mathcal{J}(\psi_i)^n$ is averaged among the three episodes. The superscript "*n*", indicates the generation number. For the sake of simplicity the notation $\mathcal{J}(\psi_i)^n$ can be abbreviated in $\mathcal{J}_i^n$.
For each *n*-generation, a Python script following the genetic operation (elitism, crossover, and mutation) spawns N_i number of individuals. The signal generator can handle connection through an RS-232 serial port, and by using a Python routine, it is possible to interface the signal generator with the genetic algorithm and automatically change amplitude and frequency. The routine was written using the PyVISA library and the queries were written with the rules and conventions of SCPI (Standard Commands for Programmable Instruments) language. The genetic algorithm also interacts with a microcontroller by using a USB serial port. As well as for the signal generator, a Python routine was written to change the delay of the microcontroller.
Once an episode with a certain triplet (ψ_i) is ended and the cost function ($\mathcal{J}_i^n$) is evaluated, the actuation signal is changed with a new triplet (ψ_{i+1}) automatically. When all individuals in a generation have been evaluated, individuals are sorted according to their performance:

$$\mathcal{J}_1^n \leq \mathcal{J}_2^n \leq ... \leq \mathcal{J}_{N_i}^n. \tag{3}$$

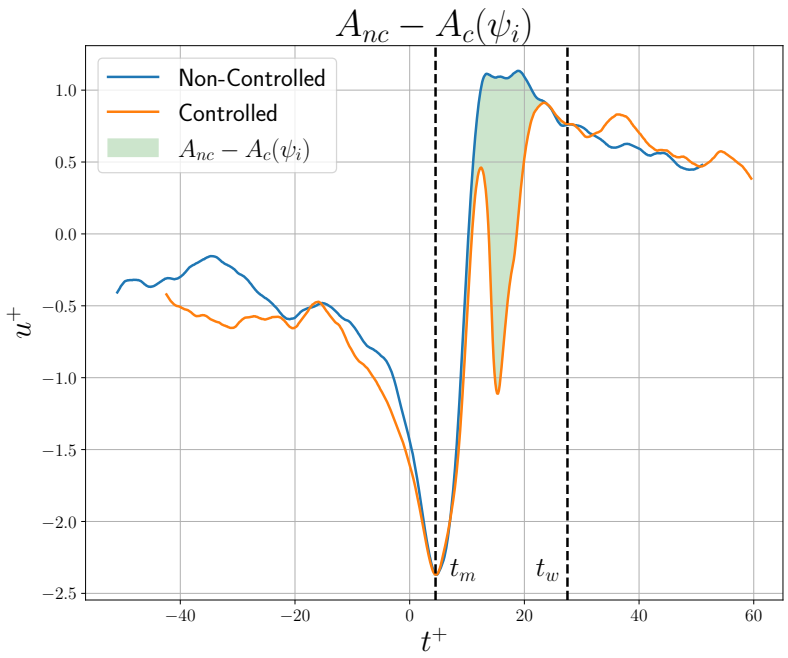

Figure 4 – Difference in the area subtended by the controlled and uncontrolled fluctuating velocity signal represented with conditional averaging. Respectively, in blue the controlled and in orange the uncontrolled velocity signal, normalized in viscous units, and in green the difference between the two curves. The box bounded by the two vertical lines represents the area in which the area is calculated.

The design of the genetic algorithm was inspired by Mendez et al. [8]. The first N_e individuals were kept for the next generation, this is called elitism. Elitism percentage M_e was set to 20%.
For each generation "*n*", the number of mutated elements was computed as follows:

$$N_{\text{mut},n} = N_{\text{gen}} M_{\text{ini}} \exp\left[\frac{n}{N_{\text{gen}}} \log\left(\frac{M_{\text{fin}}}{M_{\text{ini}}}\right)\right], \quad 0 \leq n \leq N_{\text{gen}} \tag{4}$$

where N_{gen} is the total number of generations, M_{ini} and M_{fin} are the percentage of mutation for the first and last generation respectively. M_{ini} and M_{fin} were set for the optimization respectively to 80% and to 10%.
For all remaining individuals crossover was applied. Elitism affects the percentage of individuals to be retained for the next generation. Mutation allows only a fraction of genes to be randomly replaced to allow more exploration by sampling in a uniform distribution. Crossover allows genes from two different individuals to be exchanged in equal parts. The two individuals were extracted from a triangular distribution having the individual with the lowest cost function as the peak and sorted in ascending order.
The bounds imposed on the genetic algorithm are shown in Table 1. They were chosen for both equipment limitations and operational reasons. Limitations due to instrumentation imposed a lower limit on the amplitude to $50\,\text{mVpp}$ since the signal generator (Agilent 33120A) could not reach a lower value and also a limit on the lowest achievable frequency to avoid damaging the speaker membrane. Moreover, operational limitations arose because controlling outside these ranges would result in ineffective opposition (if the delay was very high) or excessively strong control (if the amplitude was high).

Table 1 – Genetic algorithm bounds

Parameter	Lower bound	Upper bound
Frequency [Hz]	80	135
Amplitude [mVpp]	50	80
Delay time [ms]	0.15	8

Hyperparameters were tuned both to have a good convergence speed but also to avoid running into local minima.

4. Results

This section analyzes the optimization results, focusing on three key aspects: the impact of the control using the optimized parameters, the sensitivity to variations in each individual parameter, and the effect of the control at different streamwise coordinates.
In addition, the convection velocity of turbulent structures will be evaluated and the control effect on the velocity spectra will be observed.

4.1 Control parameters optimization through the genetic algorithm

The genetic algorithm optimization produced an optimal triplet for the control parameters (frequency, amplitude and delay):

$$\psi_{\text{opt}} = [96.44\,\text{Hz}, 0.066\,\text{Vpp}, 1.38\,\text{ms}]\,.$$

The first iterations of the genetic algorithm allowed an exploration of possible triplets favoring mutation. However, in the last iterations priority was given to crossover and elitism to obtain the best actuation parameters.

Table 2 – Reward value in the last generation for each triplet ψ

Frequency [Hz]	Amplitude [Vpp]	Delay [ms]	Reward value $(\text{-}\mathcal{J})$ [%]
96.44	0.066	1.38	28.99
96.65	0.061	1.27	25.63
87.94	0.066	4.77	23.69
87.43	0.066	6.46	21.73
95.09	0.075	1.94	16.94
133.88	0.063	6.46	15.66

The results obtained in the last iteration are shown in Table 2. From these data, it can be noted that even a small variation in amplitude, frequency, and delay time can yield high reward variations.
Figure 5 shows the effect of the control on the rear probe ($x^+ = 76$, $y^+ = 15$). The blue line represents the uncontrolled case, and the orange one the controlled case with ψ_{opt}. The area in green represents the positive reduction between the natural and the controlled case.
The position in which the optimal point was computed is at $x^+ = 76$ far away from the actuator. The correlation time from the detection point ($x^+ = -64$) and the actuation point ($x^+ = 0$) is approximately $2.56\,\text{ms}$ ($t^+ = 5.6$), which is longer than the optimal time imposed by the system for actuating, i.e. $1.38\,\text{ms}$ ($t^+ = 3.1$). This is because the loudspeaker actuation time and the system response time are not taken into account in the delay time. Secondly, it can be seen in Figure 5 that more effective control is achieved if action is taken prior the convected velocity gradient signal being above the threshold.
The optimized delay time, found with the genetic algorithm, enables the velocity reduction to begin precisely when the gradient of the convected structure exceeds the threshold at the detection point (dashed green line of Figure 5). The time between the detected structure on the front probe at $x^+ = -64$ (dashed black line) and the expected convected structure at $x^+ = 76$ (dashed green line) is approximately $\Delta t^+ = 12.2$.

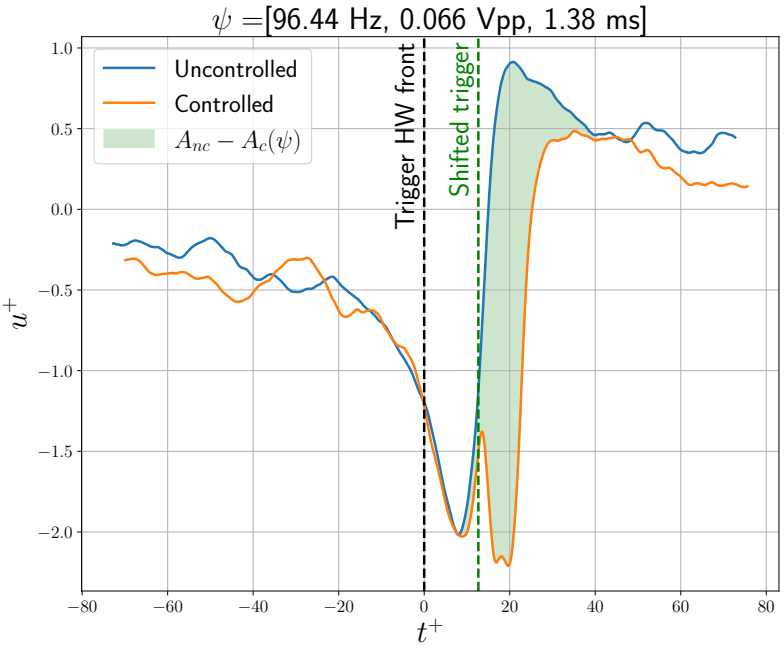

Figure 5 – Conditionally averaged sweep events detected at the rear probe ($x^+ = 76$ and $y^+ = 15$). u^+ indicates the longitudinal component of the fluctuating velocity in wall units. The dashed line in black shows the trigger coming from the front probe. The dashed line in green depicts the trigger signal delayed by Δt^+ = 12.2 which is the convection time between the front and rear probes.

4.2 Input parameters effect on the system response

It is worth observing the system's response to the actuation parameter changes. Three test cases were chosen to observe the response change.

In Figure 6, the effect of the actuation frequency can be observed. Two test cases characterized by a similar amplitude and delay time but with different actuation frequencies ($f_1 = 114\,\mathrm{Hz}$ and $f_2 = 85\,\mathrm{Hz}$) are reported. Specifically, lower frequencies allow for longer actuation times.

Figure 7, shows how the delay time imposed through the microcontroller causes the velocity reduction to be anticipated or delayed. A high delay allows reductions to occur where the velocity is the greatest; conversely, a reduced delay prevents the emergence of the velocity peak and delays its recovery. The optimal value obtained for this parameter is usually found for low delay time. However, the delay time and actuation frequency are strongly linked to obtaining a marked velocity reduction: a low delay time with a high actuation frequency does not produce positive effects because, although control occurs at the optimum point, its duration is reduced.

It can be seen clearly in Figure 8, how increasing the amplitude, for the same frequency and delay time, brings a worsening. Presumably, an increase in the amplitude increases the jet intensity. If the intensity is higher than the sweep events' vertical component, the interaction between the jet and the main flow is no longer effective in reducing the local mean velocity.

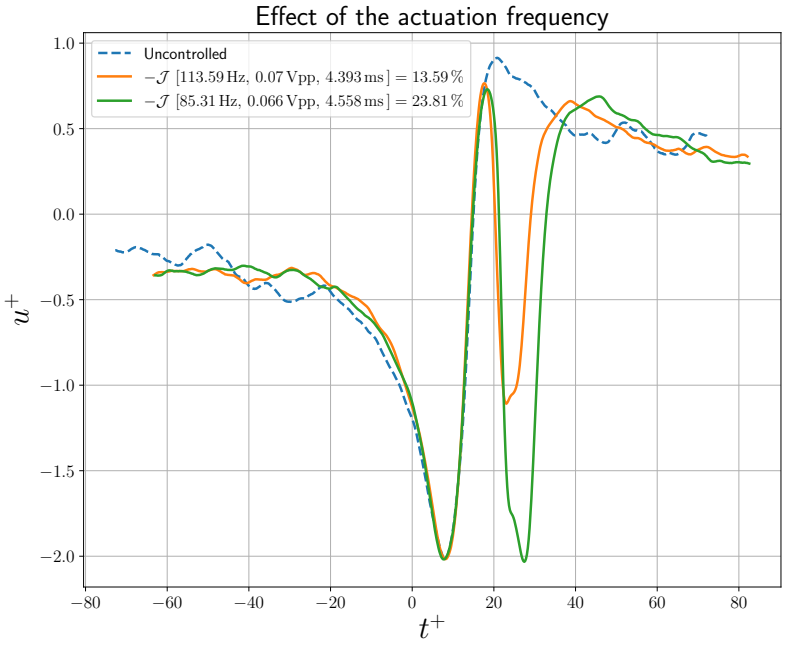

Figure 6 – Effect of the actuation frequency on the system response. The blue dashed line represents the longitudinal fluctuating component of the velocity in wall units in the uncontrolled case, the orange and the green curves represent the velocity in the controlled case with two different triplets. The percentage reward ($-\mathcal{J}$) for each triplet is shown in the legend.

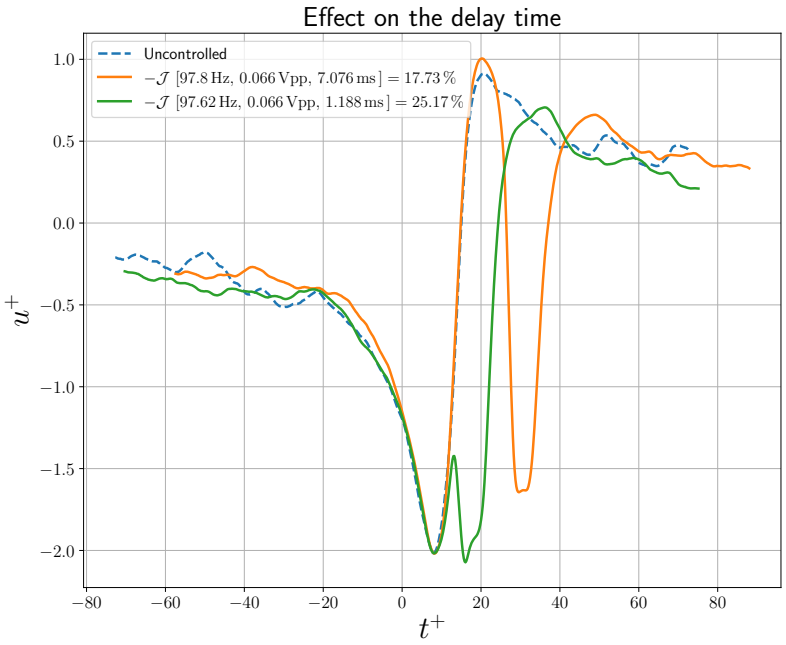

Figure 7 – Effect of the delay time on the system response. The blue dashed line represents the longitudinal fluctuating component of the velocity in wall units in the uncontrolled case, the orange and the green curves represent the velocity in the controlled case with two different triplets. The percentage reward ($-\mathcal{J}$) for each triplet is shown in the legend.

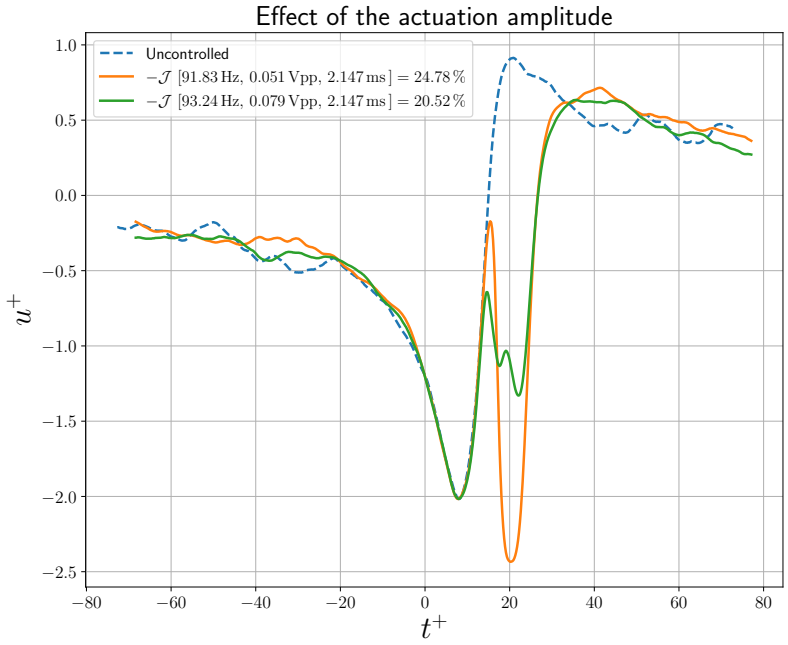

Figure 8 – Effect of the actuation amplitude on the system response. The blue dashed line represents the longitudinal fluctuating component of the velocity in wall units in the uncontrolled case, the orange and the green curves represent the velocity in the controlled case with two different triplets. The percentage reward ($-\mathcal{J}$) for each triplet is shown in the legend.

4.3 Conditional averaged analysis

The optimization of the control parameters was performed at $x^+ = 76$ and $y^+ = 15$. It is relevant to observe the effect of the control further downstream and upstream. Measurements at different streamwise locations were performed to characterize the modifications in the flow behavior when the control was active.

Figure 9 depicts the conditional averaged sweep events for different longitudinal coordinates in the controlled (with ψ_{opt}) and the uncontrolled case. Indeed, it can be observed that the events tend to decrease in intensity as the longitudinal coordinate increases, both in the natural and in the controlled case. The effect of the control becomes negligible at distances of about 500 viscous units.

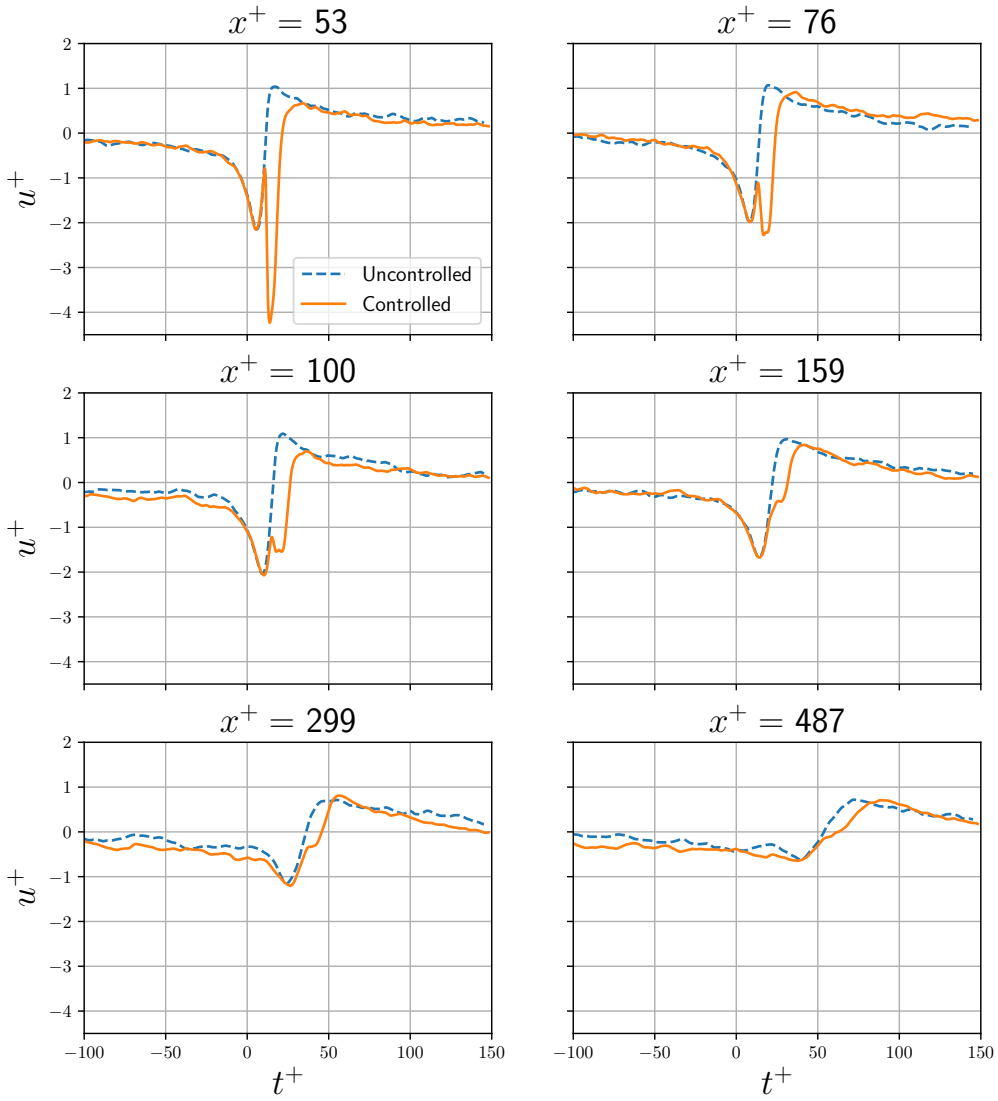

Figure 9 – Conditional averaged sweep events behavior at different streamwise locations and $y^+ = 15$. The dashed blue line represents fluctuating velocity in wall units in the uncontrolled case, and the orange line represents that in the controlled case.

4.4 Time correlation analysis

A correlation time analysis between the front and rear probe signals could be performed by sampling the signal at different downstream positions from the control point.
In Figure 10, it is possible to observe the correlation time (τ^+) as a function of the distance in viscous units (Δx^+) between the two probes. It is possible to evaluate the convection velocity in wall units (u_c^+) which is approximately 12. The same value has been found in Johansson et al. [7] for the same distance from the wall, $y^+ = 15$.

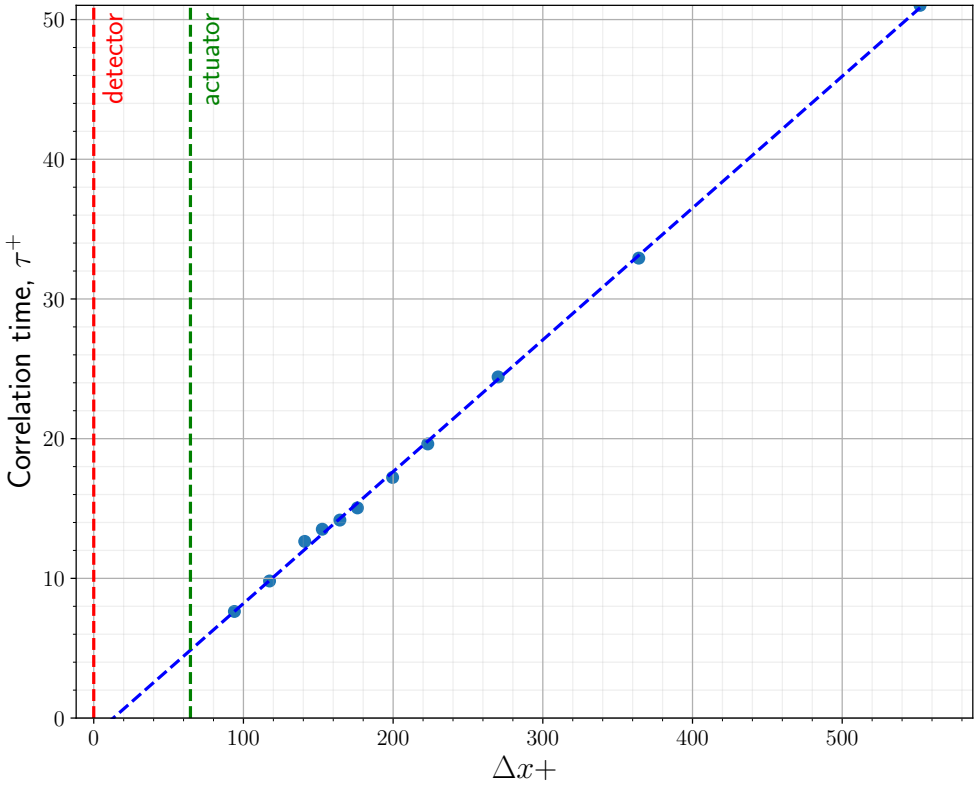

Figure 10 – Correlation time in viscous units (τ^+) as a function of the distance (Δx^+) between the front and rear probes. The distance from the wall for both probes is about 15 wall units. The red dashed line shows the position of the front probe (detector), and the green dashed line shows the position of the actuator.

4.5 Energy spectra analysis

The premultiplied energy spectra at different streamwise locations in the controlled and uncontrolled cases are depicted in Figure 11. The behavior at smaller wave numbers k is very similar between the controlled and uncontrolled cases in all the streamwise locations. This is caused by the fact that smaller wave numbers are associated with larger scale structures that are more robust and less responsive to localized control efforts. However, at the same time, the more pronounced effect of the control is apparent mostly at the smaller scales (for higher k). This effect is most significant near the control point where the influence of the control is stronger and maybe related to the loss of coherence of the flow structures.

It can be noted from Figure 11 that the energy in the spectrum turns out to be higher in the controlled case. This phenomenon is due to the fact that the control is active and feeds energy into the flow through the jet.

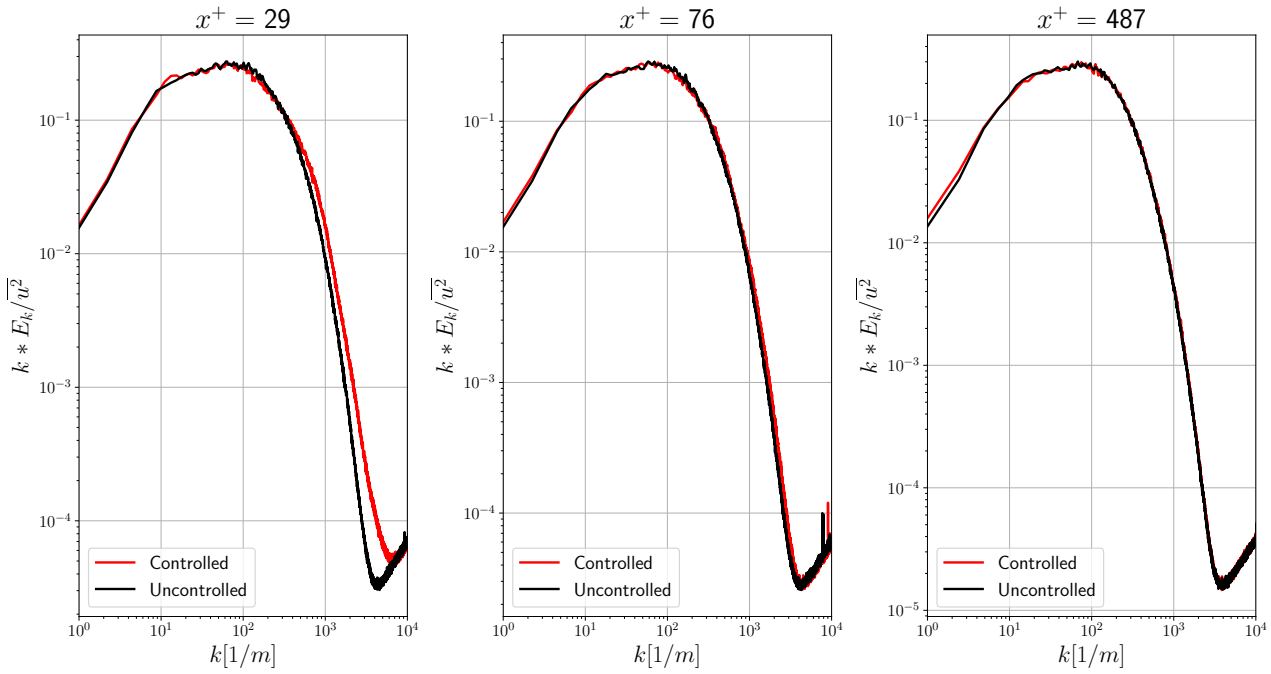

Figure 11 – Normalized premultiplied energy spectra at $y^+ = 15$ and different distances from the control point: $x^+ = 29$, $x^+ = 76$, $x^+ = 487$.

5. Conclusions

The conducted study successfully applied a genetic algorithm to optimize an opposition control strategy in a fully turbulent channel flow. The genetic algorithm identified an optimal set of control parameters, specifically the triplet $\psi_{\text{opt}} = [96.44\,\text{Hz}, 0.066\,\text{Vpp}, 1.38\,\text{ms}]$, representing frequency, amplitude, and delay time, respectively. These parameters yielded a significant reduction in the longitudinal velocity component during the sweep events, demonstrating the effectiveness of the control strategy leading to a reward up to 29 %.
Conditional analysis shows that the effect of the control last for about 500 wall units.
Energy spectra analysis shows an energy increase for higher wave numbers. This effect can be related to a loss of coherence of the flow structures caused by the interaction between the jet and the main flow.

6. Contact Author Email Address

Contact: enrico.saccaggi@polito.it

7. Acknowledgement

This publication is part of the project PNRR-NGEU which has received funding from the MUR – DM 118/2023.

8. Copyright Statement

References

[1] Blackwelder R F, and Kaplan R E. On the wall structure of the turbulent boundary layer. *Journal of Fluid Mechanics* 76, 1 (1976), 89–112.

[2] Castellanos R, Ianiro A, and Discetti S. Genetically-inspired convective heat transfer enhancement in a turbulent boundary layer. *Applied Thermal Engineering* 230 (2023), 120621.

[3] Cheng X, Qiao Z, Zhang X, Quadrio M, and Zhou Y. Skin-friction reduction using periodic blowing through streamwise slits. *Journal of Fluid Mechanics* 920 (2021), A50.

[4] Choi H, Moin P, and Kim J. Active turbulence control for drag reduction in wall bounded flows. *Journal of Fluid Mechanics* 75 (1994), 262.

[5] Dacome G, Robin M, Kotsonis M, and Baars J W. Opposition flow control for reducing skin-friction drag of a turbulent boundary layer, 2023.

[6] Di Cicca G M. Proportional opposition control of wall turbulence. In 27th *International Congress of the Aeronautical Sciences* (2010).

[7] Johansson A. V, Alfredsson P H, and Kim J. Evolution and dynamics of shear-layer structures in near-wall turbulence. *Journal of Fluid Mechanics* 224 (1991), 579–599.

[8] Mendez F J, Pasculli A, Mendez M A, and Sciarra N. Calibration of the von Wolffersdorff model using genetic algorithms, 2020.

[9] Noack B R. Closed-loop turbulence control-from human to machine learning (and retour). In *Fluid-Structure-Sound Interactions and Control* (Singapore, 2019), Y. Zhou, M. Kimura, G. Peng, A. Lucey, and L. Huang, Eds., Springer Singapore, pp. 23–32

[10] Qiao Z X, Zhou Y, and Wu Z. Turbulent boundary layer under the control of different schemes. *Proceedings of the Royal Society A: Mathematical, Physical and Engineering Sciences* 473, 2202 (2017), 20170038.

[11] Rebbeck H, and Choi K S. Opposition control of near-wall turbulence with a piston-type actuator. *Physics of Fluids* 13, 8 (08 2001), 2142–2145.

[12] Rebbeck H, and Choi K S. A wind-tunnel experiment on real-time opposition control of turbulence. *Physics of Fluids* 18 (2006), 035103.

[13] Robinson S K. Coherent motions in the turbulent boundary layer. *Annual Review of Fluid Mechanics* 23, 1 (1991), 601–639.

[14] Sonoda T, Liu Z, Itoh T, and Hasegawa Y. Reinforcement learning of control strategies for reducing skin friction drag in a fully developed turbulent channel flow. *Journal of Fluid Mechanics* 960 (2023), A30.

[15] Yu J, Fan D, Noack B R, and Zhou Y. Genetic-algorithm-based artificial intelligence control of a turbulent boundary layer. *Acta Mechanica Sinica* 37, 12 (2021), 1739–1747.